SUPPORTING INFORMATION for

Enhanced bond switching at complexion layer facilitates high fracture energy of

LATP solid-state electrolytes

Zhimin Chen[1], Tao Du[1], N. M. Anoop Krishnan[2], Morten M. Smedskjaer[1],*

[1] *Department of Chemistry and Bioscience, Aalborg University, Aalborg East 9220, Denmark*
[2] *Department of Civil Engineering, Indian Institute of Technology Delhi, Hauz Khas, New Delhi 110016, India*
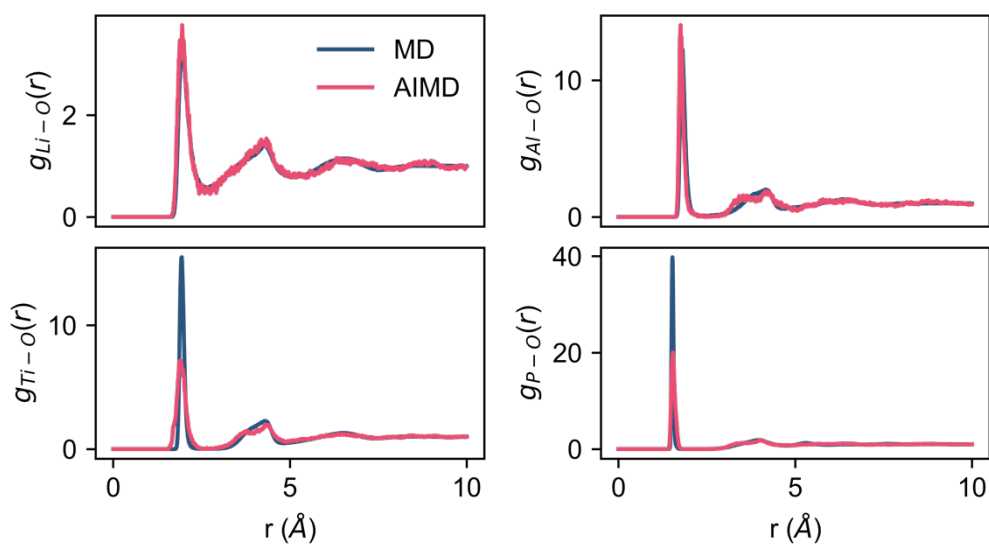* *Corresponding author. E-mail: mos@bio.aau.dk*

Supporting figures

Figure S1. Simulated partial radial distribution function of Li-O, Al-O, Ti-O, and P-O pairs obtain from the simulated LATP glasses. The glass structures of LATP are produced by both classical molecular dynamics simulations (MD) and *ab initio* molecular dynamics simulations (AIMD).
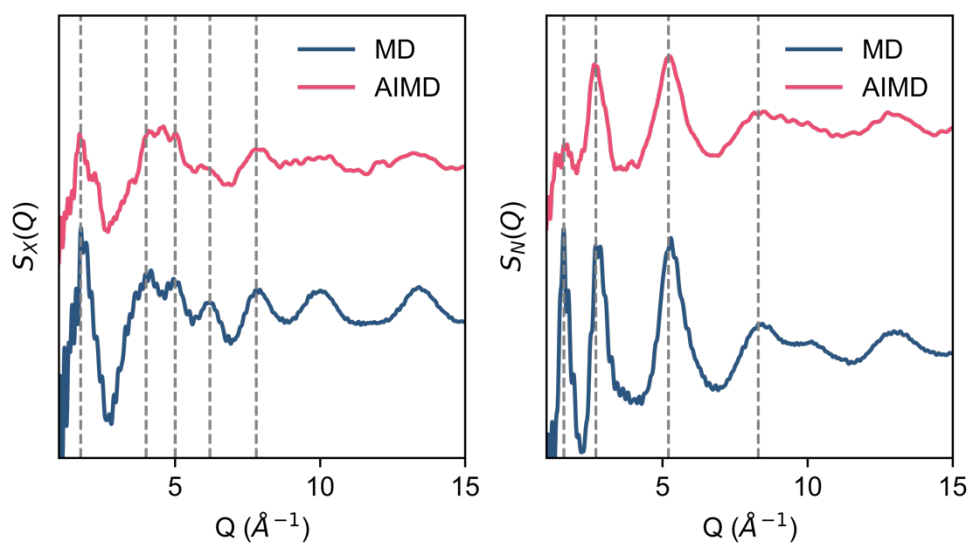
Figure S2. Simulated X-ray scattering structure factor ($S_X(Q)$, left) and neutron scattering structure factor ($S_N(Q)$, right) of LATP glasses as obtained by both classical molecular dynamics simulations (MD) and *ab initio* molecular dynamics simulations (AIMD).
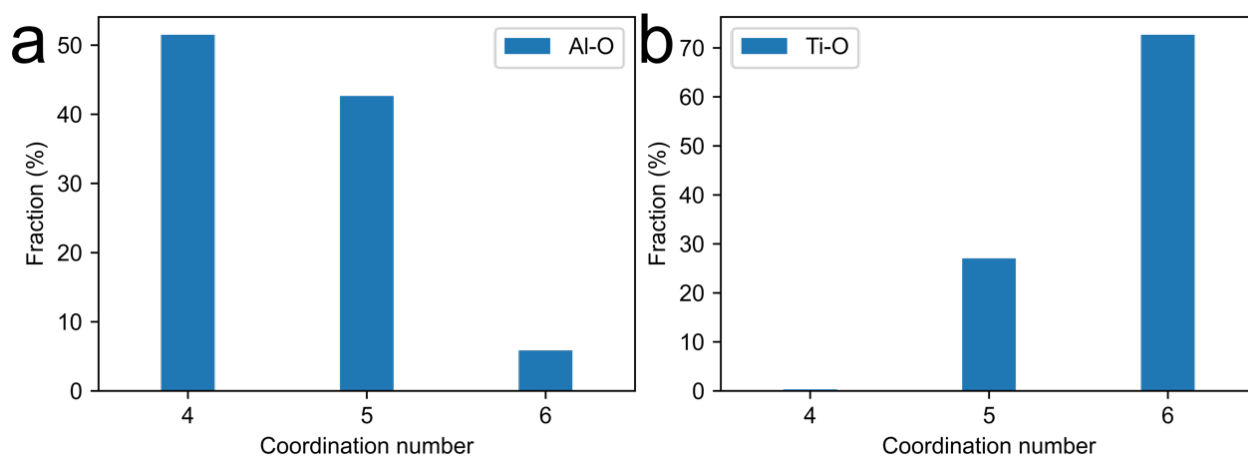
Figure S3. Histograms of coordination numbers for (a) Al-O and (b) Ti-O pairs in LATP glass.
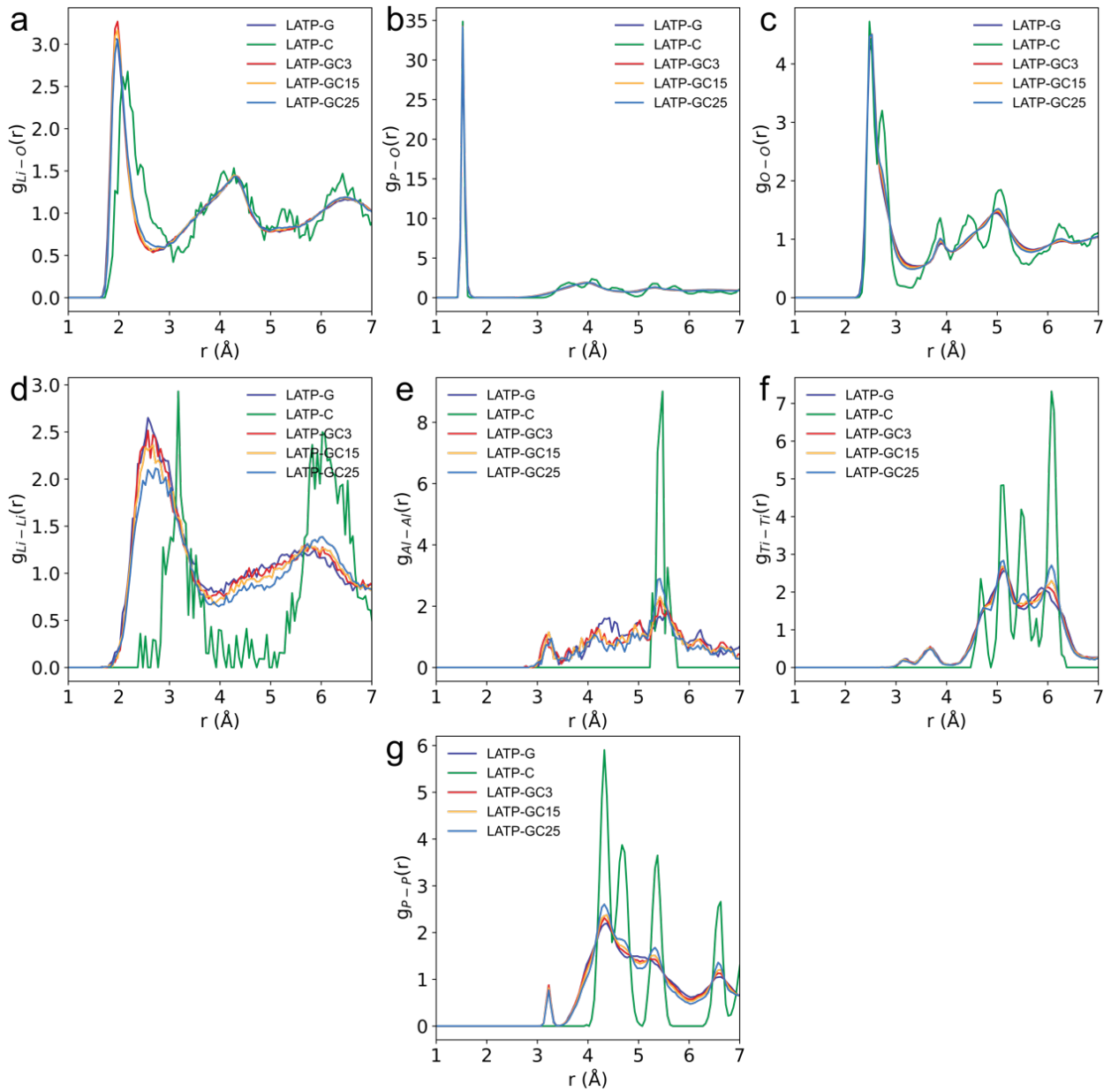
Figure S4. Partial radial distribution functions of (a) Li-O, (b) P-O, (c) O-O, (d) Li-Li, (e) Al-Al, (f) Ti-Ti, and (g) P-P pairs in the different LATP samples.
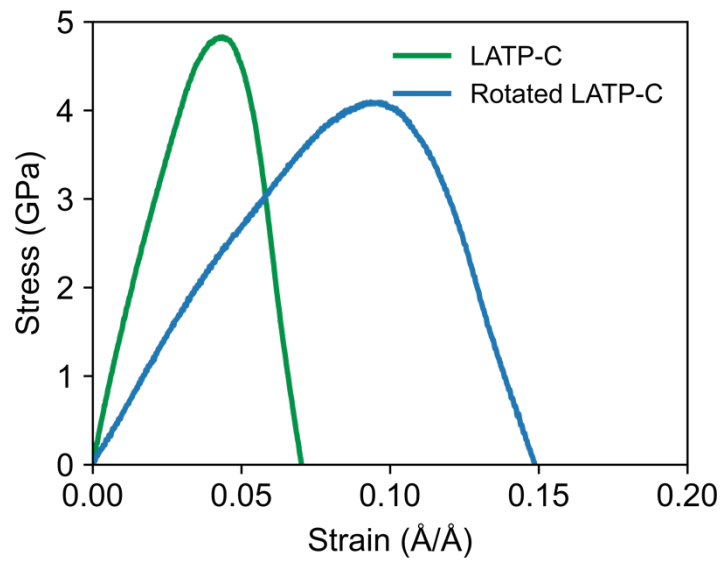
Figure S5. Stress-strain curve of the chosen orientation of LATP-C used for modeling glass-ceramics and that of the rotated LATP-C by 90 degrees.
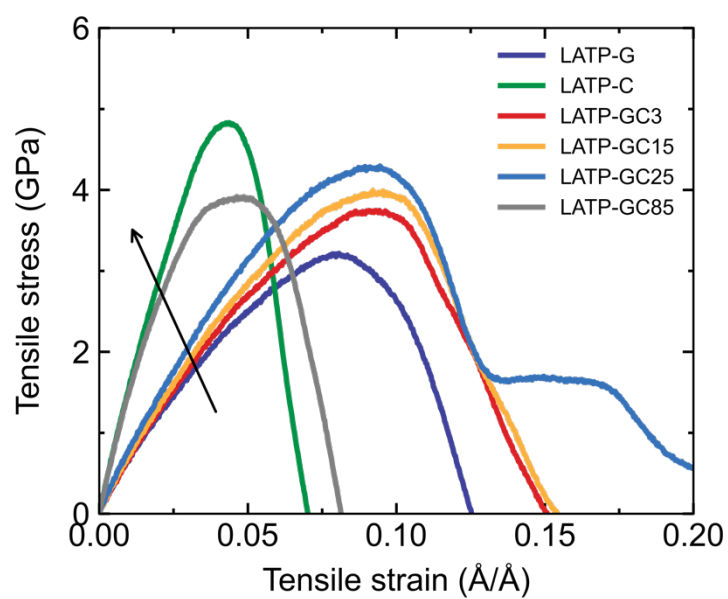
Figure S6. Stress-strain curve of simulated LATP glass-ceramics. The LATP-GC85 sample (grey line) is simulated by the combination of crystal matrix and glass phases in the glass-ceramics.
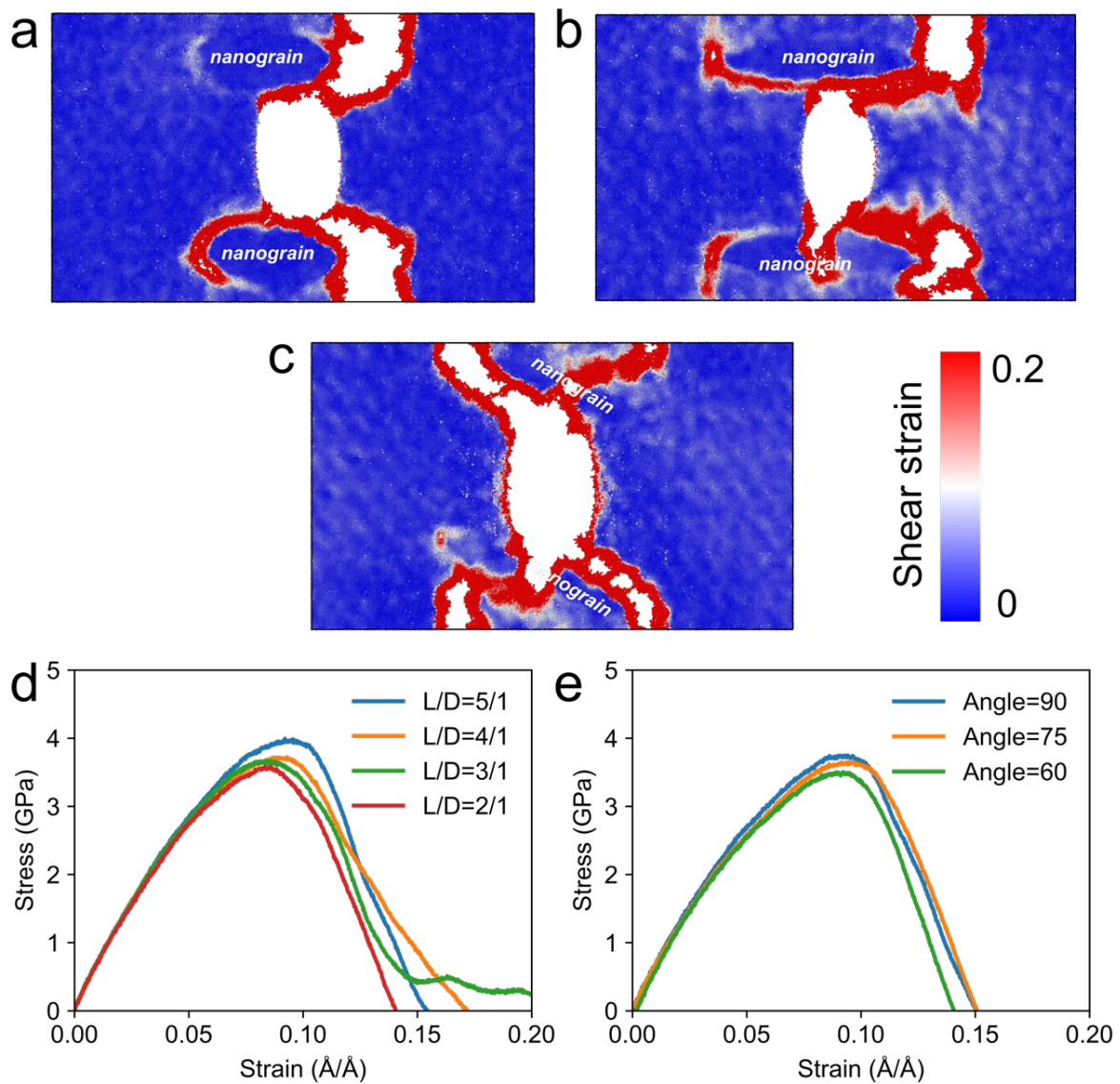
Figure S7. (a-c) Shear strain distribution of (a) LATP-GC15 with L/D = 2/1, (b) LATP-GC15 with L/D = 4/1, and (c) LATP-GC15 with an angle of 60º between nanograins and pre-crack, at the tensile strain of 0.15. (d-e) Corresponding strain-stress curves for different (d) length to diameter (L/D) ratios and (e) angles of nano-grains relative to the pre-cracks in the LATP-GC15 glass-ceramics.
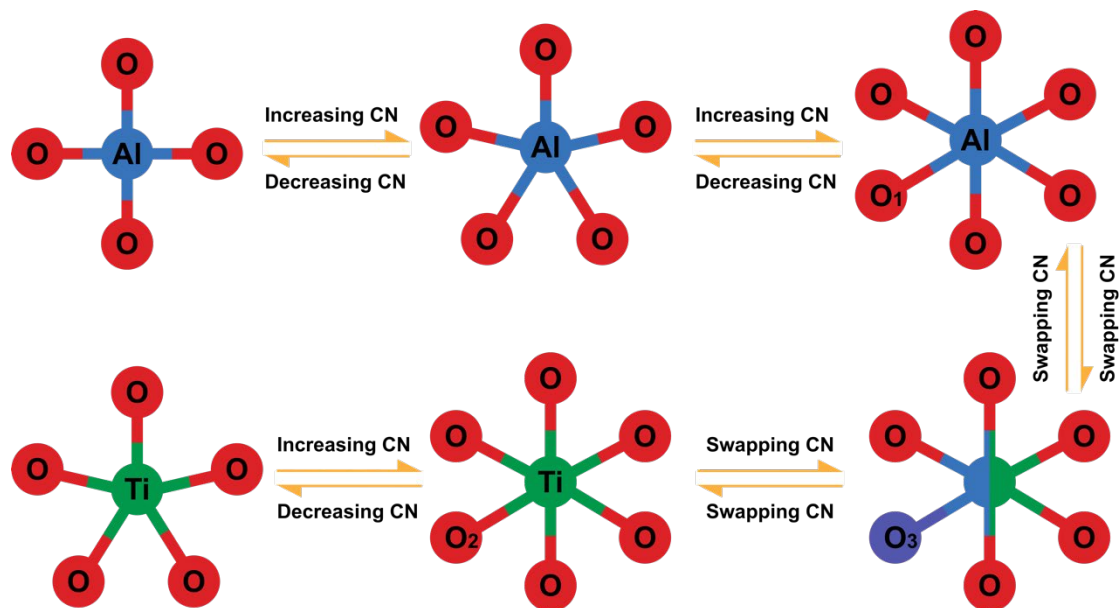
Figure S8. Schematic illustration of the investigated bond switching events of Al and Ti atoms. The decreasing coordination numbers (De), increasing coordination numbers (In), swapping coordination numbers (Sw), and unchanging coordination numbers are counted.
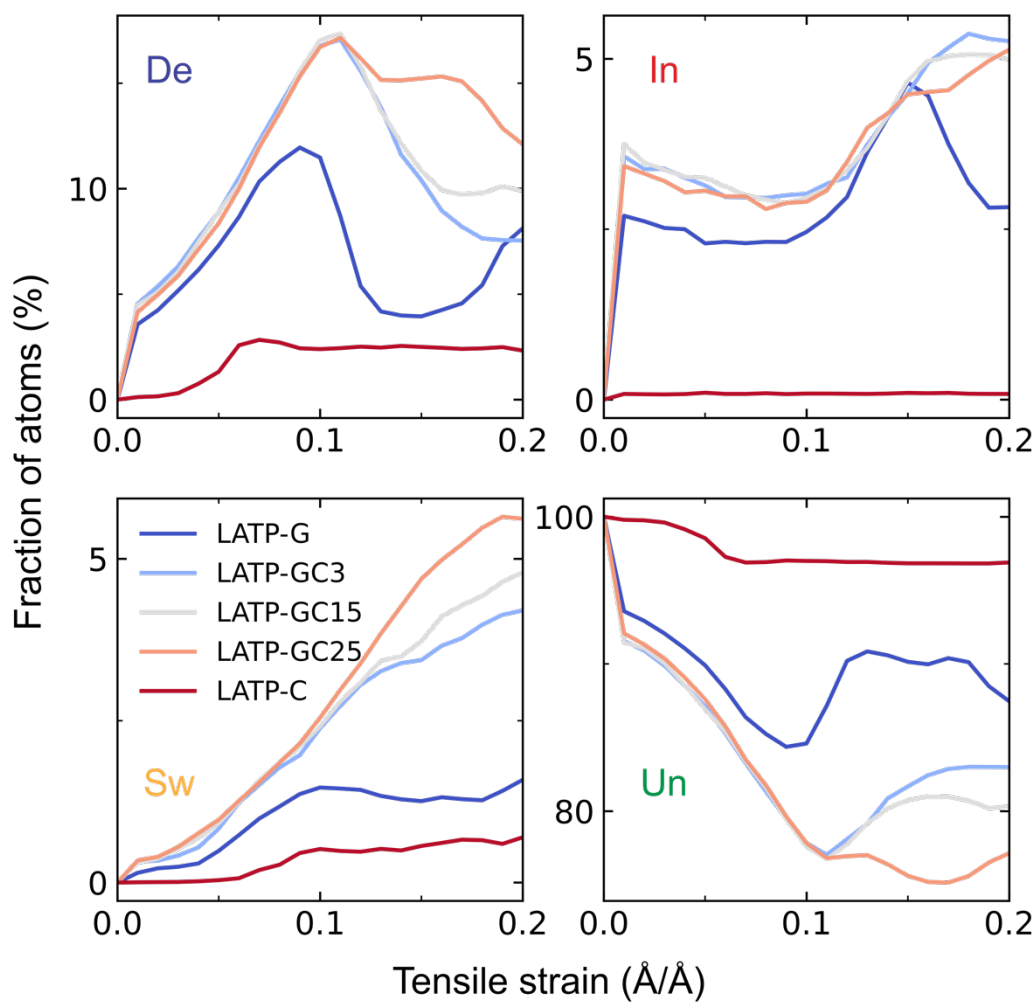
Figure S9. Fraction of bond switching events for Ti-O as a function of the tensile strain in the different LATP samples, including decreased CN (De), increased CN (In), swapped CN (Sw), and unchanged CN (Un) events.
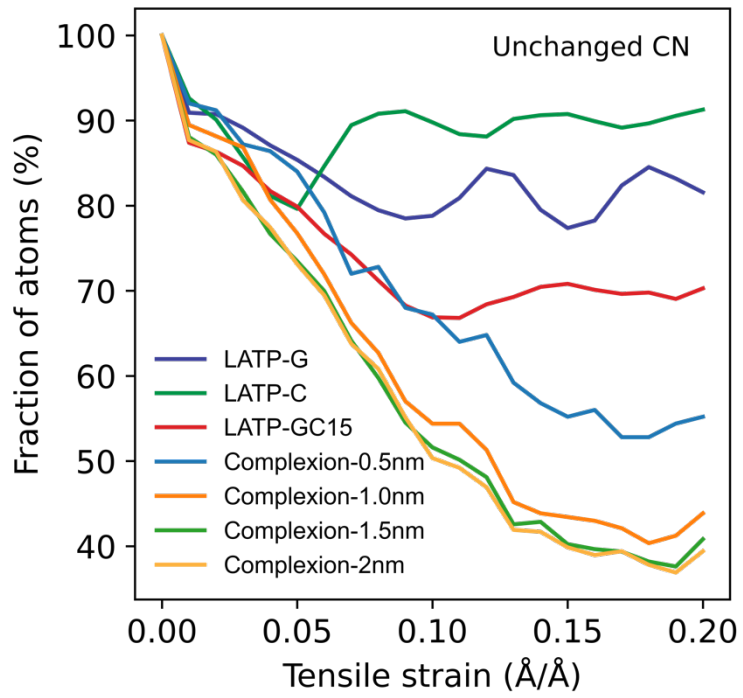
Figure S10. Fraction of unchanged bond switching events during tensile process as a function the defined thickness of complexed interface in the LATP-GC15 glass-ceramic.
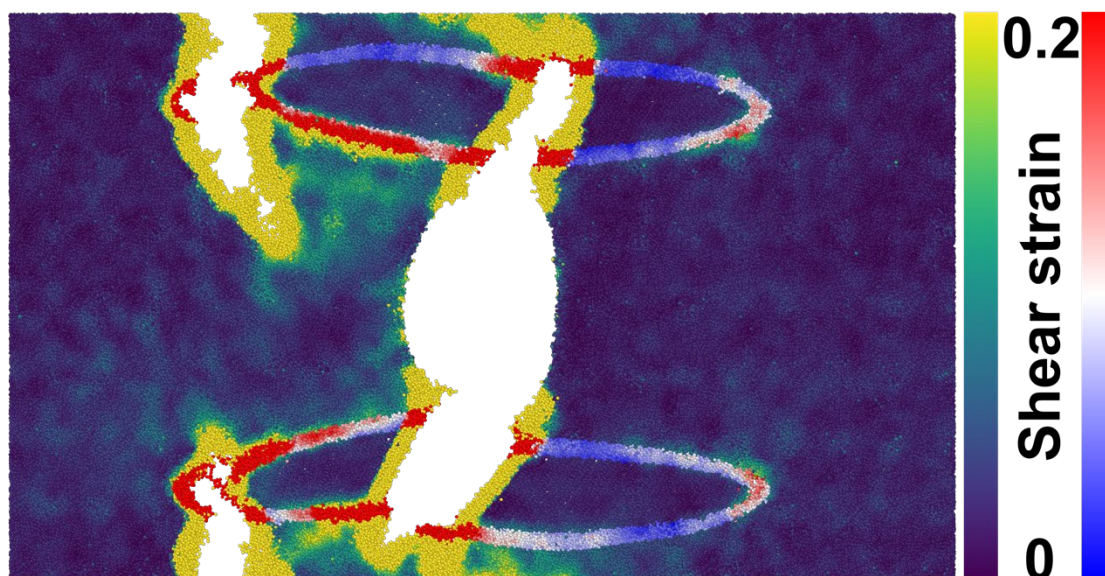
Figure S11. Shear strain distribution of the complexion interface between glass and crystal phase for LATP-GC15 glass-ceramic. The complexed interface and LATP glass-ceramic are color-coded by the shear strain values at the tensile strain of 0.15.
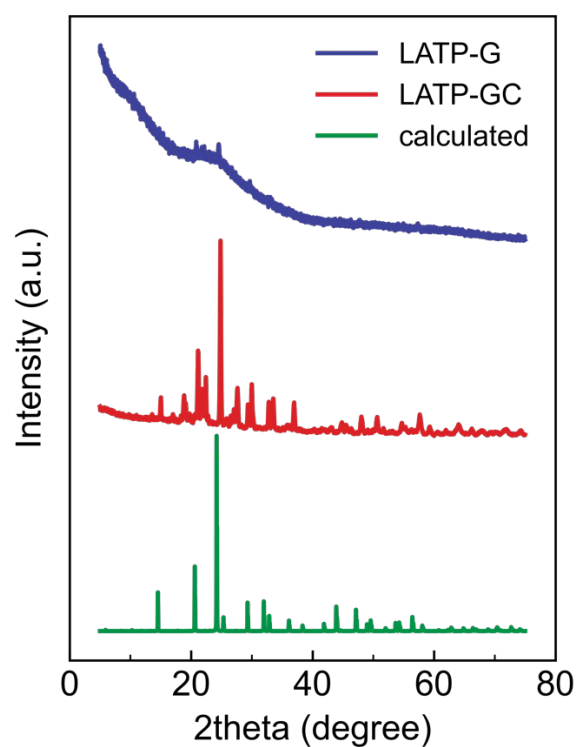
Figure S12. X-ray diffraction (XRD) pattern of experimental LATP glass, experimental LATP glass-ceramic, and calculated LATP crystal sample. The primary peaks correspond to the $Li_{1.3}Al_{0.3}Ti_{1.7}(PO_4)_3$ crystal phase.
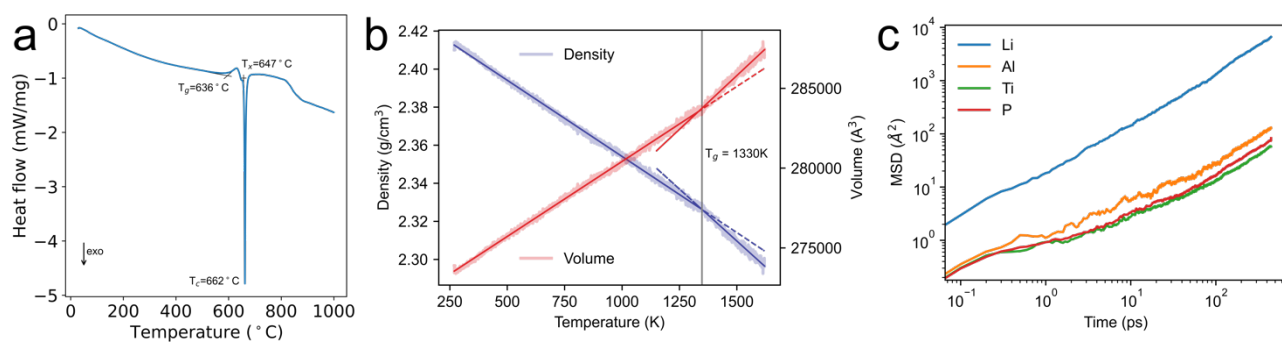
Figure S13. (a) Measured glass transition temperature (T_g) of the synthetized LATP glass electrolyte. (b) Temperature dependence of density and volume for simulated LATP glass electrolytes. The values are obtained from ten separate MD simulations. (c) Simulated mean squared displacement (MSD) of simulated LATP glass at 2300 K.
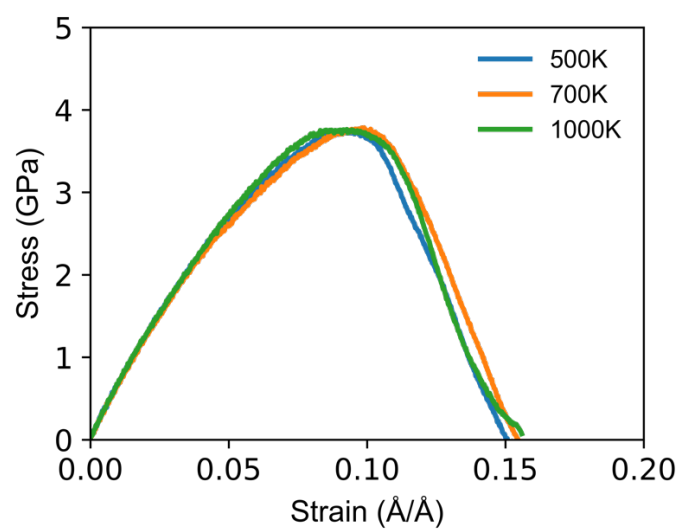
Figure S14. Stress-strain curve of simulated LATP-GC15 electrolytes annealed at different temperatures.
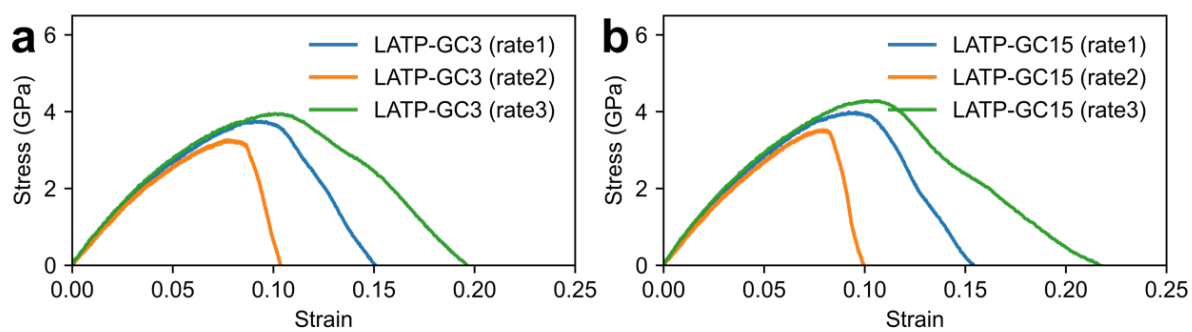
Figure S15. Effect of strain rate on the stress-strain curve for (a) LATP-GC3 and (b) LATP-GC15 samples. Rate1, rate2, and rate3 refer to strain rates of 5, 1, and 10×10^9 s^{-1}, respectively.

Supporting table

Table S1. Details on the simulated samples, where G refers to "glass", C refers to "crystal", GC refers "glass-ceramic", LD refers to "length-to-diameter ratio", and A refers to "angle relative to pre-crack".

Sample ID	Crystalline volume fraction (%)	L/D ratio (-)	Angle to pre-crack (°)
LATP-G	0	5/1	90
LATP-C	100	5/1	90
LATP-GC3	3	5/1	90
LATP-GC15	15	5/1	90
LATP-GC25	25	5/1	90
LATP-GC85	85	5/1	90
LATP-GC15-LD41	15	4/1	90
LATP-GC15-LD31	15	3/1	90
LATP-GC15-LD21	15	2/1	90
LATP-GC3-A75	3	5/1	75
LATP-GC3-A60	3	5/1	60